Publication VI

Thin Film Nano Solar Cells—From Device Optimization to Upscaling

Minna Toivola*, Timo Peltola, Kati Miettunen, Janne Halme, and Peter Lund

Helsinki University of Technology, Advanced Energy Systems, Department of Applied Physics,
P. O. Box 5100, FIN-02015 TKK, Finland

Stainless steel based dye solar cells have been upscaled from small, laboratory size test cells of 0.32 cm^2 active area to 6 cm $\times$ 6 cm "mini-modules" with active areas ca. 15 cm^2. Stainless steel works as the photoelectrode substrate whilst the counter electrode is prepared on indium-doped tin oxide coated polyethyleneterephtalate or polyethylenenaphtalate plastic foil (fluorine-doped tin oxide coated glass as a reference). Additional current collector structures were deposited on the counter electrode substrate with inkjet-printing of silver nanoparticle ink in order to reduce the lateral resistance of the plastic foil. Flexible substrates enable roll-to-roll type industrial manufacturing of the cells and the steel's superior conductivity compared to the typical substrate materials such as glass and plastic makes it possible to prepare even substantially larger modules. The best efficiencies obtained this far with the "mini-module" using a stainless steel photoelectrode are 2.5% with a platinum-sputtered indium-doped tin oxide coated polyethyleneterephtalate counter electrode and 3.4% with a thermally platinized fluorine-doped tin oxide coated glass counter electrode. These efficiencies are on the same level than those measured with small cells prepared with similar methods and materials (3.4%–4.7%, depending on configuration, which are amongst the highest reported for this kind of a dye solar cell). Replacing expensive conducting glass with steel and plastic foils as the substrate materials leads also to economical savings in the cell production.

Keywords: Dye Solar Cell, Metal Substrate, Plastic Substrate, Flexible, Upscaling.

RESEARCH ARTICLE

1. INTRODUCTION

Relatively inexpensive materials and simple manufacturing methods of nanostructured dye-sensitized solar cells (DSC)[1] have made this technology a potential alternative to the more traditional silicon and thin film photovoltaic devices. Unlike the solid semiconductor solar cells, a DSC is an electrochemical device consisting of two electrodes interconnected by a layer of redox electrolyte. Electricity is generated on the photoelectrode, which is a porous high surface area network of TiO$_2$-nanoparticles, sensitized with a light-absorbing dye, and permeated with the electrolyte. Figure 1 presents the operating principle of the DSC.

While the highest energy conversion efficiencies of small laboratory-sized test cells exceed already ten percent,[2–4] upscaling the cell size to industrially manufacturable modules and commercialization of the technology are still on an early stage. One of the main problems in making the DSC structure suitable to high throughput roll-to-roll type manufacturing is the traditionally used, rigid and fragile glass substrate. To address this issue, we have investigated a DSC geometry where the photoelectrode (PE) is deposited on stainless steel (StS) sheet. Due to steel's high conductivity (i.e., low lateral resistance on the substrate surface) employing this material as the PE substrate enables drastic enlargening of the cell size. Steel sheets withstand high temperatures, so that sintering of the PE film is possible unlike in the case of PEs deposited on plastic foils. Conducting glass is also one of the most expensive cell components, which is why replacing it with steel offers economical benefits. Further cost savings could be obtained if the DSC structure worked as a solar-active coating on building materials, e.g., roofing steels since a large part of the costs of a photovoltaic system are caused by additional supporting and installation structures of the panels.

In order to keep the cell structure completely flexible, the counter electrode (CE) has to be prepared on plastic foil, for instance ITO-PET (indium-doped tin oxide coated polyethyleneterephtalate). This poses a challenge because the sheet resistances of conductive plastics are typically so high that additional current collector structures on the

---

*Author to whom correspondence should be addressed.
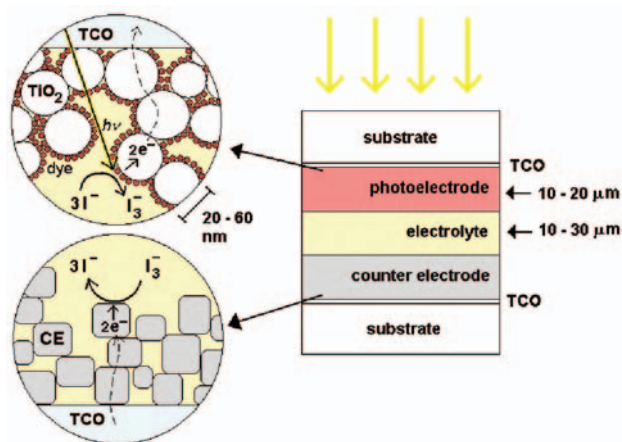
Fig. 1. Operating principle of the DSC. TCO = transparent conducting oxide.

CE substrate are needed. We have employed inkjet-printed silver nanoparticle ink stripes as the current collectors on plastic CEs and developed a semi-empirical mathematical model with which the current collector geometry can be optimized to minimize the ohmic losses caused by the CE substrate resistivity.

In a cell where the PE is deposited on opaque StS sheet light has to enter the active area through the CE and electrolyte layers. This causes optical losses which can, however, be minimized with careful optimization of the electrolyte and CE structures.

2. EXPERIMENTAL DETAILS

2.1. Cell Types

This paper presents results obtained with both small laboratory-sized test cells and larger "mini-modules." The substrate size and active area, i.e., the area of the dye-sensitized TiO$_2$ layer of the small cells were 1.6 cm × 2 cm and 0.32 cm^2, respectively, and those of the large cells 6 cm × 6 cm and 14–20 cm^2, respectively. Variation in the active area size of the large cells is due to different TiO$_2$ layer geometries (see Fig. 4). From here on, the terms "small cell" and "large cell" are used to distinguish between these two cell types.

2.2. Cell Preparation

Nanoporous TiO$_2$ photoelectrodes were prepared on StS (type 1.4301, thickness 1–1.25 mm, supplied by Outokumpu, Inc.) and on FTO (fluorine-doped tin oxide) coated glass (Pilkington TEC-15, thickness 2.5 mm, sheet resistance 15 Ω/sq., Hartford Glass Company, Inc.) substrates with doctor-blading method and high temperature sintering, using commercial titania paste (Sustainable Technologies International). StS was chosen amongst several other metal materials because it did not corrode in the

electrolyte.[5] Electrode film thickness was 10–15 μm and the films were sensitized overnight in 0.32 mM ethanol solution of the N719 dye (cis-bis(isothiocyanato)bis(2,2′-bipyridyl-4,4′-dicarboxylato)-ruthenium(II) bis-tetrabutyl-ammonium, Solaronix SA). Counter electrodes were prepared on FTO glass substrates with the standard thermal platinization method[6] and on ITO-PET and ITO-PEN (indium-doped tin oxide coated polyethylenenaphtalate) plastic foils (sheet resistances 60 Ω/sq. and 15 Ω/sq., supplied by Bekaert, Inc. and Peccell, Inc., respectively) with 1–2 nm of sputtered platinum as the catalyst. Conductive polymer PEDOT (poly(3,4-ethylenedioxythiophene)) was also studied in this purpose but possible stability problems with it made sputtered Pt a more reliable alternative. Since glass is the typical DSC substrate for both electrodes, the glass electrodes were used as a reference against which the performance of the plastic CE and StS PE cells were compared. With small cells, the StS sheets were employed also as the CE substrates (PEs on glass in this geometry) and catalyzed by thermal platinization, analogously to glass CEs.

The electrodes were sealed together on a hot plate at 100–110 °C using thermoplastic Surlyn ionomer resin film as a spacer and sealant after which the cells were filled with either liquid or semi-solid (gel) electrolyte. The liquid electrolyte composition was 0.5 M LiI, 0.03 or 0.05 M I$_2$, and 0.5 M 4-*tert*-butylpyridine in 3-methoxypropionitrile. Semi-solid electrolyte, which was employed in some of the small cells, was made of the liquid by gelatinizing it with 5 wt% of PVDF-HFP (polyvinylidenefluoride-hexafluoropropylene).[7] More detailed descriptions of the cell preparation can be found in our previous publications.[5, 8]

The iodine (and consequently, triiodide) concentration of 0.03 M (which differs from the typical 0.05 M of the standard DSC electrolyte) is optimized for a cell where the light enters the active area through the CE and the electrolyte layers: Since triiodide absorbs strongly on visible wavelengths, it is responsible for the most of the optical losses in the electrolyte. However, because the diffusion of the triiodide ions limits the current flow in the electrolyte, due to their smaller concentration compared to other charge carriers, and because the order of the maximum current the cell is able to generate is known, the definition of the diffusion limited current density[9] can be used to find an optimal combination of the electrolyte layer thickness and a corresponding triiodide concentration.

The small and large cells were prepared analogously, except for the additional current collector stripes that were inkjet-printed on the large cells' CE substrates using commercial silver nanoparticle ink (Advanced Nano Products). The width of the stripes was 1–1.5 mm and the height varied from 2.5 μm to 7 μm, depending if one or two layers of ink were printed. To protect the ink stripes from the electrolyte (triiodide ions corrode many metals,

including silver) 3 mm wide strips of Surlyn thermoplastic film were melted on top of the stripes. Figures 2 and 3 present the schematics and a photograph of the small cells, respectively, and Figures 4 and 5 the TiO₂ layer and current collector geometries and a photograph of large cells, respectively. Because the sheet resistance of ITO-PET is larger than that of the FTO glass or ITO-PEN, the amount of the current collector stripes is larger in the ITO-PET CE cell, which also narrows the TiO₂ "finger" width and lessens the active surface area. Additional widenings on the CE's main current collector side of the stripes help to minimize the ohmic losses even further. Large cells were prepared also with a "fingerless" TiO₂ layer geometry, as a reference against which the effect of the additional current collectors could be compared.

2.3. Measurements

The cell performance was characterized with current density–voltage (I–V) measurements in a solar simulator. The custom-built simulator consists of ten 150 W halogen lamps, a temperature-controlled measurement plate and a calibrated monocrystalline silicon reference cell with which the lamps can be adjusted to provide the standard 100 mW/cm² illumination intensity. The spectral mismatch factor of the simulator, defined with the reference cell and the measured spectral irradiance of the halogen lamps is used to make the curves correspond with the standard AM1.5G equivalent illumination.

2.4. Model for the Large Cell

In order to find the optimal CE current collector geometry to minimize the resistive losses in the cell, a semi-empirical mathematical model was developed.[10] The model is based on partial differential equations describing the current flow in the cell and a slightly "expanded" standard solar cell equivalent circuit. The model takes into account the real cell geometry, dimensions and materials, in a form of varying electrode surface conductivity, depending on the surface material (StS, glass, ITO-PET/PEN, silver nanoparticle ink).

If the current flow in the cell is assumed ohmic, the continuity equation for the CE is

$$\frac{\partial \rho}{\partial t} - \sigma \nabla^2 V_{CE} = S \qquad (1)$$
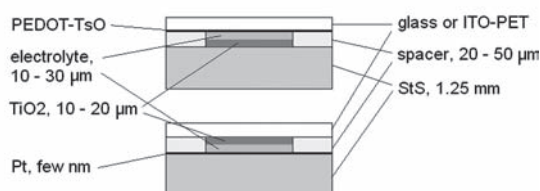
Fig. 2. StS-based small cell geometries. Upper: StS as the PE (here with a PEDOT-catalyzed CE) substrate. Lower: StS as the CE substrate.
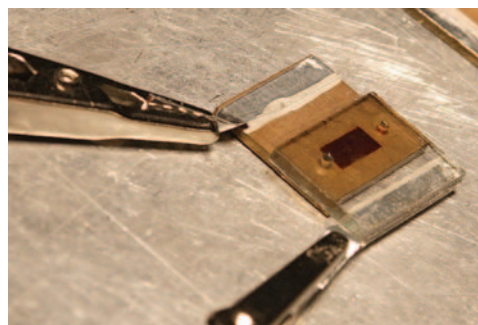
Fig. 3. Photograph of a small StS PE cell (here with a glass CE).

and for the PE

$$\frac{\partial \rho}{\partial t} - \sigma \nabla^2 V_{PE} = -S. \qquad (2)$$

In Eq. (1) and (2), ρ is the charge density, σ the surface conductivity, V_{CE} the CE potential, V_{PE} the PE potential, and S the current source. Because the electrolyte layer is only few tens of micrometers thick, compared to the centimeter-scale dimensions of the electrode surface, the cell can be treated as two-dimensional, which leads to certain simplifications, i.e., current flow is strictly perpendicular to the electrode surface. Also, in the case of StS PE cells, the StS surface resistivity can be approximated to zero, compared to the resistivities of the other cell components, which means $V_{PE} = 0$ and it is enough to model only the CE side. The PE current generation, on the other hand, can be modelled as an "infinite" number of parallel current generators behaving like an infinitesimally small DSC. Figure 6 illustrates this "expanded" solar cell equivalent circuit. Current generation at the PE is described as a parallel connection of a photocurrent source and a diode, modelling the current generation by the dye and the recombination (leakage/dark current) of the electrons in the TiO₂ layer with the oxidized form of the dye and the electrolyte species.

In general, the source term in the Eqs. (1) and (2) is the sum of the photo- and diode currents I_{ph} and I_D, respectively:

$$S = I_{ph} - I_D \qquad (3)$$
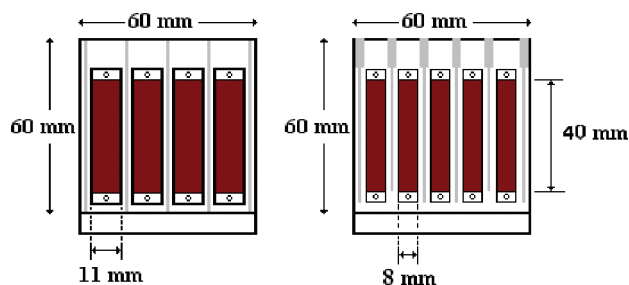
Fig. 4. TiO₂ layer (red) and current collector (grey) geometries of the large cells with StS PEs. Left: a large cell with a glass/ITO-PEN CE. Right: a large cell with an ITO-PET CE.
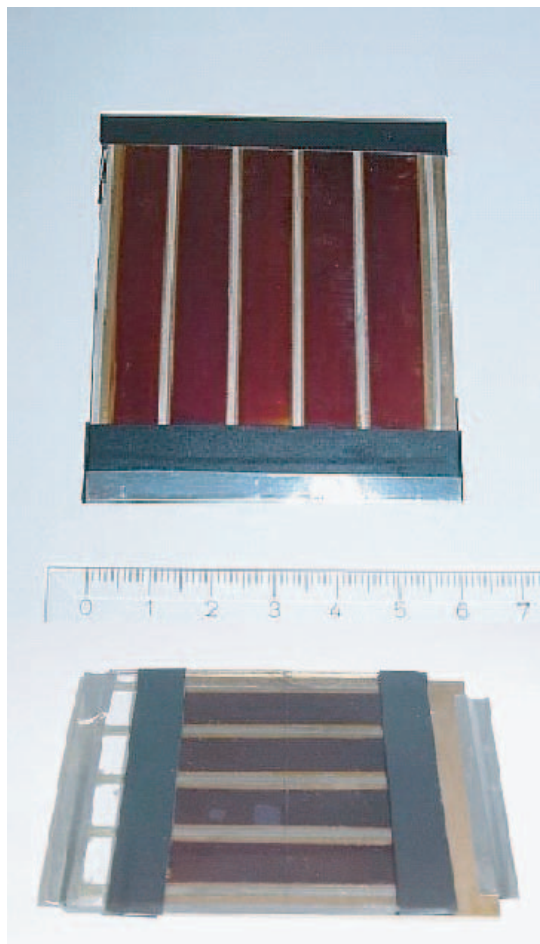
Fig. 5. Photograph of large StS PE cells (upper: ITO-PET CE; lower: glass CE). Aluminum tapes on the edges of the cells, perpendicular to the inkjet-printed silver stripes work as the main current collectors.

but because the diode current term (based on approximation of Butler-Volmer type charge transfer at the electrode)

$$S = I_{ph} - I_0 e^{\alpha z F(V_{CE}+R_{el}S-V_{PE})/(RT)} \quad (4)$$

where I_0 and α are constants, z the number of electrons transferred in the electrode reaction (two in this case), and R_{el} the electrolyte resistance, includes the source term in itself, S needs to be solved numerically. This can be done
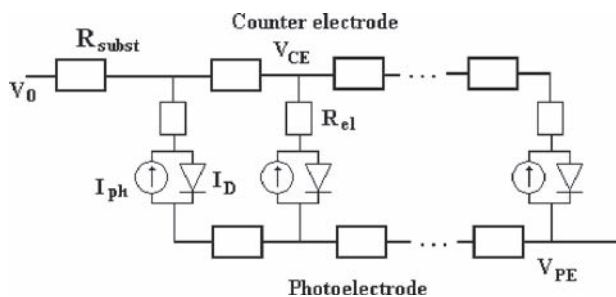
Fig. 6. DSC equivalent circuit, including the substrate and electrolyte resistivities and the current source term.

$$1: \quad \sigma\nabla^2 V_{PE} = 0$$

$$2: \quad \sigma\nabla^2 V_{PE} = I_{ph} - I_1 e^{m_1(V_{CE}-V_{PE})} - I_2 e^{m_2(V_{CE}-V_{PE})} - I_3 e^{m_3(V_{CE}-V_{PE})}$$

$$A: \quad (-\sigma\nabla V_{PE})\cdot\bar{n} = 0$$

$$B: \quad V_{PE} = V_0$$
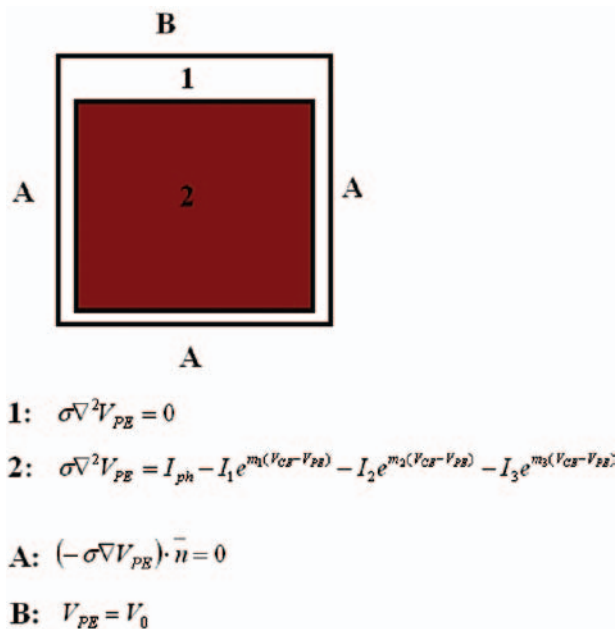
Fig. 7. An example of the modelled geometries: A large DSC with "fingerless" TiO$_2$ layer. 1 and 2: Current flow equations; A and B: Boundary conditions.

by fitting Eq. (4) to a measured $I–V$ curve of a small cell (short circuit current is a good first approximation for I_{ph}), which gives values for the parameters I_0, α and R_{el}, and then calculating numerically some points of an $S–V$ curve, after which a simpler equation for S can be fitted to that curve. In this study, source term of the form

$$S = I_{ph} - I_1 e^{m_1(V_{CE}-V_{PE})} - I_2 e^{m_2(V_{CE}-V_{PE})} - I_3 e^{m_3(V_{CE}-V_{PE})} \quad (5)$$

where I_1, I_2, I_3, m_1, m_2, and m_3 are empirical parameters, was used in the $S–V$ curve fitting and inserted into Eqs. (1) and (2) (equations were assumed time-independent).

To make the model realistic, boundary conditions must also be set. As depicted in Figure 7, current can flow only through the main current collector (edge "B"), and the other edges of the cell are treated as simple insulators. Electrodes are treated as constant value potentials and the $I–V$ curve of the cell is obtained by changing the value of the potential difference between the PE and the CE. The model was solved with COMSOL Multiphysics finite element method solver (COMSOL, Inc.) and verified before use by comparing measured and modelled small cell $I–V$ curves.

3. RESULTS AND DISCUSSION

3.1. Small Cell Performance

Table I lists the best $I–V$ parameters (short circuit current I_{sc}, open circuit voltage V_{oc}, fill factor FF, and energy conversion efficiency η) of small StS-based DSCs, included

Table I. *I–V* parameters of the StS-based cells versus the standard DSC configuration.[11]

Cell type	I_{sc} (mA/cm^2)	V_{oc} (V)	*FF* (%)	η (%)
1	14.0	0.704	0.58	5.8
2	13.6	0.663	0.40	3.6
3	12.2	0.675	0.57	4.7
4	12.4	0.618	0.57	4.3
5	11.8	0.597	0.54	3.8
6	10.9	0.638	0.49	3.4

Cell types: 1: glass PE, liquid electrolyte with 0.05 M I$_2$, Pt-glass CE (standard DSC configuration, included as a reference). 2: glass PE, liquid electrolyte with 0.05 M I$_2$, Pt-StS CE. 3: StS PE, liquid electrolyte with 0.03 M I$_2$, Pt-glass CE. 4: StS PE, gel electrolyte with 0.03 M I$_2$, Pt-glass CE. 5: StS PE, gel electrolyte with 0.03 M I$_2$, Pt-sputtered ITO-PET CE.[11] 6: StS PE, liquid electrolyte with 0.05 M I$_2$, Pt-sputtered ITO-PET CE (a configuration comparable to the large cells). *Source:* Reprinted with permission from [11], M. Toivola et al., *Proceedings of the NSTI Nanotech Nanotechnology Conference and Trade Show*, June, Boston, U.S.A. (**2008**). © 2008.

here as a reference against which the large cell performance could be compared. With electrolyte optimization, i.e., reducing the electrolyte layer thickness from 50 μm to 20 μm and the iodine concentration from 0.05 M to 0.03 M we were able to gain 16% increase in the cell efficiency and 26% reduction in the optical losses.[11, 12]

The StS PE cell configuration was chosen for further research and cell size upscaling. This is because the performance of the StS CEs was not satisfactory and also because, in order to keep the cell completely flexible, the PE in the StS CE cell should be prepared on plastic. Plastic can not withstand sintering temperatures, 450–500 °C, which leads to plastic PEs' poorer performance and weaker mechanical stability, in comparison to sintered PE films. StS PEs, on the other hand, gave almost as good efficiencies as the PEs deposited on glass, as can be seen from Figure 5 (StS and glass PEs, glass CEs and gel electrolyte). Compared to literature, the efficiencies obtained with our uncoated StS PE (i.e., StS without an additional protective layer under the PE film) cells are amongst the highest reported.[13, 14]

The unsatisfactory performance of the StS CEs can be explained with larger charge transfer resistance on the StS CE–electrolyte interface, compared to that measured with a glass CE. This increases the series resistance of the cell and shows for example as a lower fill factor. In our previous research it was also noticed that the adhesion of thermally deposited Pt on StS is not as good as on FTO glass.[5]

This can lead to inefficient charge transport and additional resistive losses between the catalyst film and the substrate.

3.2. Modelling of the Large Cell

The effect of the substrate surface and current collector stripe resistivities on the cell performance was calculated with the model with five different combinations of substrate sheet resistances, setting the silver stripe resistance (R_s) to 0 Ω/m, 30 Ω/m and 50 Ω/m in turn for each calculation. Sheet resistance combination 0/15 Ω/sq. corresponds to a cell with a StS PE and FTO glass or ITO-PEN CE, 0/60 Ω/sq. to a StS PE and ITO-PET CE, 15/15 Ω/sq. to an all-glass or all-ITO-PEN substrate cell, and 60/60 Ω/sq. to an all-ITO-PET cell. Combination 0/0 Ω/sq. was included as an "ideal cell" reference against which the efficiency losses caused by the substrate and silver stripe resistances could be compared. Cell efficiencies were calculated from the simulated *I–V* curves of a 20.21 cm^2 active area cell, setting the generated photocurrent to 8 mA/cm^2, which is a realistic value for a large cell. Simulation results are summarized in Table II.[10]

From Table II it can be seen how the efficiency losses caused by the substrate sheet resistance and silver stripe resistance follow approximately linear behavior (efficiency loss of a 60/60 Ω/sq. combination is approximately four times more than that for 15/15 Ω/sq. substrates). Simulation results also suggest that lowering the substrate resistance as low as possible is not, after all, the most critical factor in order to produce high efficiency cells: For example, the efficiency of a glass CE cell (0/15 Ω/sq. combination) is still more than 90% and even that of an ITO-PET CE cell (0/60 Ω/sq. combination) more than 80% of that of the "ideal" cell. This indicates there are other issues than the substrate resistivity that tend to restrict the large cell efficiencies.

Uneven voltage losses and correspondingly, uneven current generation in the cell were some of the efficiency-limiting factors that could be identified with the model. Figure 8 presents the modelled voltage losses and current density in a 6 cm × 6 cm DSC.

Voltage loss and current density distribution in Figure 8 are easily explained with spatial effects. Total resistive losses on the substrate surface and in the current collector stripes grow the longer the electrons have to travel before they reach the main current collector (located on top of the

Table II. Cell efficiencies and efficiency losses calculated with different substrate sheet and silver stripe resistance combinations.

Substrate sheet resistances Ω/sq.	η ($R_s = 0$ Ω/m) (%)	η ($R_s = 30$ Ω/m) (%)	η ($R_s = 50$ Ω/m) (%)	η loss ($R_s = 0$ Ω/m) (%)	η loss ($R_s = 30$ Ω/m) (%)	η loss ($R_s = 50$ Ω/m) (%)
0/0	3.32	n/a	n/a	0.00	n/a	n/a
0/15	3.24	3.11	3.02	0.08	0.21	0.30
0/60	2.96	2.83	2.75	0.37	0.49	0.57
15/15	3.14	2.89	2.74	0.18	0.43	0.58
60/60	2.60	2.38	2.25	0.72	0.94	1.07
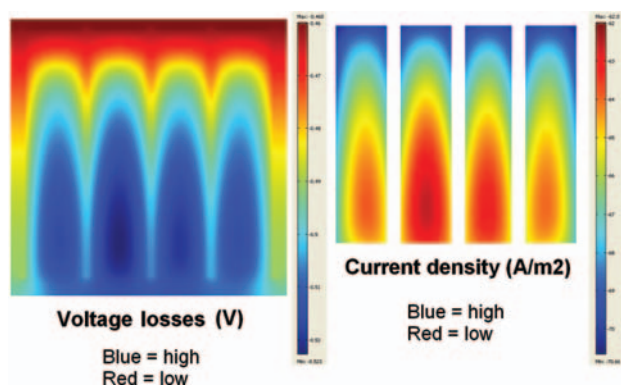
Fig. 8. Modelled voltage loss and current generation distribution in a 6 cm x 6 cm DSC. Main current collector is located on the top of the picture.

pictures in Fig. 8), so total voltage loss is also larger the farther from that the electricity is generated. This is something that can not be totally avoided in a large DSC but its efficiency-lowering effect can be minimized with optimization of the TiO₂ finger width and the current collector geometry, which was also done with the model.

The optimal TiO₂ finger widths were 1.1 cm for a StS PE and glass/ITO-PEN CE cell and 0.8 cm for a StS PE and ITO-PET CE cell whilst the finger length was set at 4.7 cm. It was also calculated that a few millimeters' deviation from the optimal width reduced the efficiency less than 5%, which leaves the PE geometry suitably tolerant to natural variations in repeatability, especially when the cells are prepared by hand. The final PE geometries are presented in Figure 4 (in real cells, the TiO₂ finger length was further reduced to 4.0 cm to leave enough room for the main current collectors on the top and bottom edges of the cell). In order to reduce the ITO-PET's sheet resistance enough, it was calculated that the current collector stripe's own resistivity must be under 60 Ω/m. This was obtained with two layers of inkjet-printed silver nanoparticle ink, which resulted in stripe resistivities of 23–30 Ω/m.

3.3. Large Cell Performance

Efficiency values of the real cells were very close to those obtained with simulations. Table III presents the *I–V* parameters and the best efficiencies measured with large, 6 cm × 6 cm substrate DSCs.[10] All cells in Table III had StS photoelectrodes and liquid electrolyte.

The reason for the ITO-PEN CE cell's poorer performance remains open this far, but it is possible that the cell was partly short-circuited or that the quality of the current collector stripes or their adherence to the substrate was not as good as with other cells (lower *FF* measured with the ITO-PEN CE indicates larger total resistance of the cell)—only a very few ITO-PEN CE cells were prepared and the current collector stripes were printed in a different batch than those on other CE substrates. Almost 3.5% efficiency obtained with a large glass CE cell and even

Table III. *I–V* parameters of the best 6 cm × 6 cm DSCs with different CE substrate materials.

Active area cm²	Counter electrode	Catalyst	I_{sc} (mA/cm²)	V_{oc} (V)	FF (%)	η (%)
14.58	FTO-glass	Thermal Pt	8.94	0.64	59.18	3.38
15.88	ITO-PET	Sputtered Pt	8.41	0.58	50.85	2.46
14.60	ITO-PEN	Sputtered Pt	6.55	0.61	43.68	1.73

the 2.5% with an ITO-PET CE cell are very good, however, especially when compared to the values of small cells manufactured with same materials and methods (Table I), even though this comparison must be made with some caution. Due to capillary forces, flexible plastic foils tend to bend towards the opposite substrate if the area between the sealant stripes is wide enough, like in the case of large area plastic CE cells. This changes the optical properties of the cells and the amount of light entered to the PE through the CE and electrolyte layers. Errors caused by this should be small enough though to justify the comparison of the orders of the efficiency values.

The main problem in the preparation of the large cells was protection of the CE current collector stripes from the electrolyte. Whilst the Surlyn strips worked in this purpose, their deposition, especially by hand, was time-taxing and in order to ensure no electrolyte leaking under the strip, they had to be kept quite wide (3 mm), which efficiently reduced the current-generating active area. Tests to replace the Surlyn strips with inkjet-printed polymer films–which would also greatly simplify the CE preparation since both the current collector and protective layer deposition could be done with the same equipment–are currently under way, along with further enlargement of the cell size and semi-automated cell manufacturing.

4. SUMMARY AND CONCLUSIONS

We have successfully upscaled the stainless steel based dye solar cell from small, 0.32 cm² active area laboratory test cell to 6 cm × 6 cm "mini-module" with active area of ca. 15 cm², keeping the cell efficiency on the same level than that measured with the small cells, i.e., 3.4% with a StS PE and FTO glass CE and 2.5% with a StS PE and ITO-PET CE (4.7% and 3.4% with small cells prepared on the same substrates, respectively). Inkjet-printing of silver nanoparticle ink turned out to be a viable method to prepare additional current collector structures on the CE substrate to reduce the CE's lateral resistance. On the PE such structures are not needed due to steel's superior conductivity when compared to other substrate materials.

Room for improvement in the efficiencies still exists. Flexible substrate materials allow cost-efficient roll-to-roll type industrial manufacturing of the cells, however, and the additional cost savings when glass substrates are replaced with steel and plastic foils, together with the possibility to integrate this kind of a DSC directly to building materials

lead to economically feasible manufacturing of even lower efficiency cells.

References and Notes

1. B. O'Regan and M. Grätzel, *Nature* 353, 737 (**1991**).
2. M. Grätzel, *Curr. Appl. Phys.* 6, e2 (**2006**).
3. M. K. Nazeeruddin, P. Pechy, T. Renouard, S. M. Zakeeruddin, R. Humphry-Baker, P. Comte, P. Liska, L. Cevey, E. Costa, V. Shklover, L. Spiccia, G. B. Deacon, C. A. Bignozzi, and M. Grätzel, *J. Am. Chem. Soc.* 123, 1613 (**2001**).
4. M. K. Nazeeruddin, T. Bessho, L. Cevey, S. Ito, C. Klein, F. De Angelis, S. Fantacci, P. Comte, P. Liska, H. Imai, and M. Grätzel, *J. Photochem. Photobiol. A: Chem.* 185, 331 (**2007**).
5. M. Toivola, F. Ahlskog, and P. Lund, *Solar Energy Mater. Solar Cells* 90, 2881 (**2006**).
6. N. Papageorgiou, W. Maier, and M. Grätzel, *J. Electrochem. Soc.* 144, 876 (**1997**).
7. P. Wang, S. Zakeeruddin, and M. Grätzel, *J. Fluorine Chem.* 125, 1241 (**2004**).
8. M. Toivola, L. Peltokorpi, J. Halme, and P. Lund, *Solar Energy Mater. Solar Cells* 91, 1733 (**2007**).
9. A. Hauch and A. Georg, *Electrochim. Acta* 46, 3457 (**2001**).
10. T. Peltola, Special assignment, Helsinki University of Technology (**2008**).
11. M. Toivola, K. Miettunen, J. Halme, and P. Lund, *Proceedings of the NSTI Nanotech Nanotechnology Conference and Trade Show*, June, Boston, U.S.A. (**2008**).
12. M. Toivola, K. Miettunen, J. Halme, F. Ahlskog, and P. Lund, *Proceedings of the 21st European Photovoltaic Solar Energy Conference and Exhibition*, September, Dresden, Germany (**2006**).
13. M. Kang, N.-G. Park, K. Ryu, S. Chang, and K.-J. Kim, *Solar Energy Mater. Solar Cells* 90, 574 (**2006**).
14. Y. Jun, J. Kim, and M. Kang, *Solar Energy Mater. and Solar Cells* 91, 779 (**2007**).

RESEARCH ARTICLE